Available online at www.sciencedirect.com
SCIENCE DIRECT®
ELSEVIER
International Journal of Multiphase Flow 29 (2003) 1685–1717
International Journal of Multiphase Flow
www.elsevier.com/locate/ijmulflow

A model for simulating gas bubble entrainment in two-phase horizontal slug flow

M. Bonizzi, R.I. Issa *

Department of Mechanical Engineering, Imperial College, Exhibition Road, London SW7 2BX, UK

Received 8 January 2003; received in revised form 1 September 2003

Abstract

In an earlier paper it was shown that the basic one-dimensional transient two-fluid model is capable of capturing horizontal and near-horizontal slug flow automatically. However, that work did not account for the effect of gas entrainment into the liquid slug body which is deemed to be an important phenomenon. In this paper, a mathematical model to account for the entrainment of gas bubbles into liquid slugs is proposed, implemented and validated. The model is cast in the framework of the existing two-fluid model and is incorporated in a computational procedure, which is applied to the prediction of slug flow in horizontal and slightly inclined pipes. The model entails the introduction of a scalar equation for the transport of the dispersed gas bubbles within the liquid. The rate of entrainment of gas at the slug front is supplied as a closure relation, the expression for which is obtained from existing correlations. The model is validated against experimental data and the comparison shows satisfactory agreement. However, the inclusion of the aeration model appears to yield marginal differences when compared to predictions which ignore entrainment in the horizontal pipe flow cases studied. More significant differences are obtained in the case of the flow in a V-section pipeline.

Keywords: Slug flow; Gas bubbles entrainment; Numerical simulation; Two-fluid model

1. Introduction

In slug flow, gas is often entrained from the large elongated gas (often called Taylor) bubble into the liquid slug and this is thought (if not taken for granted) to have a significant effect on the

* Corresponding author. Fax: +44-20-78238845.
E-mail address: r.issa@imperial.ac.uk (R.I. Issa).

0301-9322/$ - see front matter
doi:10.1016/j.ijmultiphaseflow.2003.09.001

slug behaviour. It is hence desirable to model this phenomenon in order to understand its importance as well as to improve the accuracy of the prediction of slug characteristics. The present study is focused on the modelling of this gas bubble entrainment (also referred to as "aeration") and its effects on liquid slugs in horizontal gas–liquid flow in pipes.

In the previous work of Issa and Kempf (2003), it was demonstrated that the one-dimensional transient two-fluid model is capable of capturing slug initiation and development automatically. Numerical simulations were made starting from unstable stratified flow in which instabilities could grow to bridge the pipe and form slugs. The simulations showed that the phenomenon can be simulated by the model, and that continuous trains of slugs could be generated automatically. The resulting predictions for some of the main characteristics of slug flow compared favourably with experimental data. However, that model ignored the phenomenon of small-bubble entrainment from the large elongated bubbles preceding the liquid slug. This was thought to be the reason behind some of the observed discrepancies in the prediction of the overall hold-up. The model proposed here is an extension of the work of Issa and Kempf and is based on the introduction of a scalar-transport equation for the volume fraction of the entrained dispersed bubbles in the liquid slug. The momentum equation for the liquid phase is replaced by one for the mixture of liquid and entrained bubbles. Thus the resulting model retains the same framework as that of the standard two-fluid model.

The physical mechanism which leads to gas entrainment in horizontal and nearly horizontal two-phase slug flow is quite complex, and only few experiments have been carried out in order to arrive at a thorough understanding of it. The work by Jepson (1987) helped to shed some light and showed that the physical process of slug aeration is very similar to that of air bubble entrainment in hydraulic jumps. Jepson (1987) studied a stationary slug, by forming a hydraulic jump that bridged the pipe and observed the resulting bubble entrainment into the liquid from the gas ahead of it. He suggested that the phenomenon is analogous to the entrainment of small gas bubbles into the body of slugs occurring in slug flow and this would result from the fragmentation of the tail of the elongated Taylor bubble into small gas pockets that are entrapped in the flowing liquid (Chanson, 1996). This is a direct consequence of the strong turbulent action induced by the large vortex motion set up by the entrance of the liquid film at the slug front (Fernandes et al., 1983), as is depicted in Fig. 1. Using flash and cine photography, Jepson (1987) observed the formation of pulses of gas bubbles in the liquid slug, and found that the pulse frequency increases with increasing liquid impingement velocity. Moreover, part of the air which is entrained across the jump, returns to the Taylor bubble ahead of it. Thus, the net rate of gas entrainment is the result of a balance between bubble injection and rejection. The slug aeration would therefore correspond

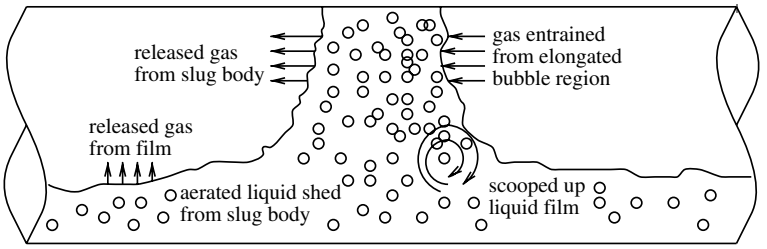

Fig. 1. Aerated slug unit.

to swarms of bubbles formed in the mixing region, which then detach from the mixing vortex, like what happens in a hydraulic jump, where the action of the vortex (often called the "roller"), breaks the free surface ahead of the jump, leading to air packets entering the jump (Chanson, 1996). The pick-up process that occurs at the slug front (Fan et al., 1993), seen in a frame of reference travelling at the slug front velocity, is akin to a plunging jet (the liquid film) entering a stationary pool (the slug body) (Bonetto and Lahey, 1993). Several authors found that when this liquid jet exceeds a critical velocity, small bubbles from the elongated bubble are entrained in the slug (Bonetto and Lahey, 1993; Manolis, 1995; Grotjahn and Mewes, 2001; Andreussi and Bendiksen, 1989). Concurrently, aerated liquid sheds from the slug body into the trailing film (Dukler and Hubbard, 1975).

In most cases, the aeration of the liquid film under the elongated bubble was found to be negligible since buoyancy tends to drive the dispersed bubbles up leading to de-aeration of the liquid film. Bendiksen et al. (1996) however, observed a much higher slug void fraction in air–oil slug flow than in air–water flow. This is probably due to higher degree of aeration of the liquid film in air–oil systems, thereby contributing to a higher gas entrainment rate into the slug.

The distribution of dispersed gas in the slug (referred to as slug void fraction α_B in the present work) depends on flow rates, pipe diameter, pressure, pipe inclination, and fluid properties (Bendiksen et al., 1996). In horizontal air–water slug flow, the dispersed gas bubbles are usually homogeneously distributed over the cross-section at the slug front. The bubbles migrate to the top of the pipe further along the body of the slug. If the flow rates are high, almost uniform distribution of gas bubbles over the whole slug length occur (Bendiksen et al., 1996). For intermediate flow rates, the gas fraction decreases along the slug (Andreussi et al., 1993). Fabre and Liné (1992) observed the stratification of small bubbles in liquid slugs due to buoyancy (overcoming turbulent dispersion effects).

Aeration increases with slug velocity, and can only be neglected, if the slug velocity is sufficiently low (Nydal and Banerjee, 1996). One example of the dependency on physical properties is the influence of the surface tension. For a constant Froude number and increasing Eötvös number, the void fraction in the slug increases, and the surface tension decreases. Hence, surface tension is an important factor in the break-up of the interface between the elongated bubble and the slug front (Fabre and Liné, 1992).

The effect of gas entrainment in liquid slugs plays an important role in determining the flow characteristics. The void fraction within the liquid slug during the entrainment process can be very high (Ferschneider, 1983). Fabre and Liné (1992) estimated that the void fraction in liquid slugs can be up to 25%. Sudden instabilities and level surges can occur, such that slug growth and collapse can become quite different from un-aerated slug flow. One major effect is the break-up of large slugs into smaller ones (Nydal and Andreussi, 1991). As a consequence, slug frequency, mean liquid hold-up, and slug body length become strongly dependent on the entrainment process.

The most common approach for incorporating gas entrainment in slug flow calculations is the use of empirical correlations for the dispersed bubble void fraction in the slug. Common relations are those of Gregory et al. (1978) and Andreussi and Bendiksen (1989). Gregory et al. (1978) measured the liquid volume fraction in the body of the slug using capacitance-type liquid volume fraction sensors in a light oil–air system in 25.8 and 51.2 mm diameter pipes. They correlated their results in terms of the mixture velocity U_M only as:

$$\alpha_{Ls} = \frac{1}{1 + (U_M/8.66)^{1.39}}, \tag{1}$$

where, in the slug body, the fundamental relation:

$$\alpha_B = 1 - \alpha_{Ls} \tag{2}$$

holds.

Malnes (1982) proposed an alternative correlation also based on the same data of Gregory et al. (1978) as:

$$\alpha_{Ls} = 1 - \frac{U_M}{C_c + U_M}, \tag{3}$$

where C_c is a dimensional coefficient defined as:

$$C_c = 83\left(\frac{g\sigma}{\rho_L}\right)^{0.25}, \tag{4}$$

and σ is the gas–liquid surface tension. Among the different expressions for the slug hold-up, the one given by Andreussi and Bendiksen (1989), who studied air entrainment into water slugs using two transparent Plexiglas tubes of 50 and 90 mm internal diameter and 17 m in length, has been found to be the most accurate over a wide range of experimental conditions. Their correlation is based on the assumption that, the net rate of gas bubble entrainment in the body of the slug is given by a mass balance between the bubble production and loss rate, as was shown by Jepson (1987). Their correlation is given by:

$$\alpha_{Ls} = 1 - \frac{U_M - u_{mf}}{U_M + u_{m0}} \tag{5}$$

with

$$u_{mf} = 2.6\left[1 - 2\left(\frac{D_0}{D}\right)^2\right]\sqrt{gD}, \quad D_0 = 2.5 \text{ cm}, \tag{6}$$

$$u_{m0} = 2400\left[1 - \frac{1}{3}\sin\beta\right]Bo^{-3/4}\sqrt{gD}, \tag{7}$$

$$Bo = \frac{\rho_L g D^2}{\sigma}. \tag{8}$$

Recently Abdul-Majeed (2000), using his own data consisting of 435 slug hold-up points taken from seven different sources, has proposed a new correlation in order to compute the slug void fraction, which only depends on the fluid viscosities and mixture velocity:

$$\alpha_{Ls} = 1.009 - \left(0.006 + 1.3377\frac{\mu_G}{\mu_L}\right)U_M. \tag{9}$$

Most, if not all, of the available correlations for the average slug void fraction in liquid slugs were found to be unsatisfactory when applied to different geometries from those used in extracting the empirical correlations (Paglianti et al., 1992). This deficiency is reinforced by the results of the

present study. This is perhaps not surprising since the above mentioned correlations are derived from fully developed slug flow, and do not account for the transient behaviour of slug growth and collapse.

Alternative modelling approaches involve the application of correlations (also empirical) for the entrainment rate (Nydal and Andreussi, 1991; Manolis, 1995). This approach can be implemented directly as a closure law in 1D slug models (Bendiksen et al., 1996) as is indeed done here. The above approaches exist in various combinations and degrees of sophistication.

To obtain a detailed and dynamic representation of the gas volume fraction distribution in the slug, the present study employs an additional scalar-transport equation for the volume fraction of gas bubbles in a slug body, which fits within the framework of the two-fluid model. The momentum and continuity equations for the liquid phase are now taken to stand for the mixture of liquid and dispersed small bubbles rather than for pure liquid as is normal with the standard two-fluid model. In these equations, the mixture density replaces that of the pure liquid.

2. The model

The standard two-fluid model is based on the formulation of two separate sets of conservation equations for the balance of mass, momentum and energy for each of the phases (Wallis, 1969; Ishii, 1975). The transfers of mass, momentum, and energy between the two phases, and between the fluids and the walls, are included via source terms and must be formulated using correlations (Ishii and Mishima, 1984; Jones and Prosperetti, 1985).

Compared to the two-fluid model for un-aerated flow (Issa and Kempf, 2003), the present model accounts for mass transfer between the gas and liquid phases, taking place both at the slug front, where gas bubbles are entrained from the elongated bubble, and at the slug tail, where gas bubbles leave the slug to enter the next gas bubble (see Fig. 1). This is achieved simply by treating the *aerated* liquid (which now contains a dispersion of small gas bubbles) as a single mixture phase, while retaining the gas as the second phase. At present, the model accounts for gas bubble entrainment in the slug body region only, assuming therefore that the liquid film is free of bubbles. In fact the aeration of the liquid film under the elongated bubbles is neglected in most slug flow models and this is a valid assumption for horizontal and slightly inclined air–water flows, since buoyancy tends to de-aerate the liquid film. However, this assumption is not an essential feature of the model, and can easily be dispensed with if necessary.

The model requires the introduction of one additional transport scalar equation for the bubble concentration within the liquid mixture. The adopted approach employs the drift-flux concept (Zuber and Findlay, 1965; Ishii, 1978), wherein the mixture of liquid and gas bubbles is treated as a single phase, and the two phasic velocities are retrieved from the velocity of that mixture by means of a scalar equation for the slip velocity.

It is easy to show (Bonizzi, 2003) that the liquid and centre of mass velocities are practically identical in a fully dispersed flow with high liquid to gas density ratios. Thus, the liquid and bubble velocities may be expressed as:

$$u_{\mathrm{L}} \approx u_{\mathrm{M}} \tag{10}$$

and

$$u_B \approx u_M + u_s, \tag{11}$$

respectively. In the above equations, the subscripts L, B, and M relate to liquid, gas bubble, and the mixture respectively, while u_s represents the slip velocity between the gas bubbles and liquid:

$$u_s = u_B - u_L. \tag{12}$$

The following quantities are now defined: α_L is the volume fraction of the liquid component (un-aerated) at any point, α_G is the volume fraction of the gas phase flowing separately, i.e. in the stratified region, α_B is the volume fraction of the gas bubbles entrained in the slug body, and α_M stands for the volume fraction of the mixture of liquid and dispersed (i.e. entrained) gas bubbles. The compatibility equation which needs to be enforced therefore is that between α_M and α_G and is given by:

$$\alpha_M + \alpha_G = 1. \tag{13}$$

Thus in the slug body, $\alpha_G = 0$ and $\alpha_M = 1$. Amongst the mixture, liquid, and dispersed bubbles, the following relationship holds:

$$\alpha_M = \alpha_B + \alpha_L. \tag{14}$$

Thus, in un-aerated liquid, $\alpha_B = 0$ and $\alpha_M = \alpha_L$.

Finally the mixture density ρ_M is given by:

$$\rho_M = (1 - \alpha_B)\rho_L + \alpha_B \rho_G. \tag{15}$$

The gas is treated as a compressible fluid and its density is calculated from the ideal gas law; the liquid is assumed to be incompressible.

When the above assumptions are introduced, the governing equations for an isothermal transient one-dimensional stratified and aerated slug flow become:

- gas continuity equation:

$$\frac{\partial(\rho_G \alpha_G)}{\partial t} + \frac{\partial(\rho_G \alpha_G u_G)}{\partial x} = -\dot{m}_B, \tag{16}$$

- mixture continuity equation:

$$\frac{\partial(\rho_M \alpha_M)}{\partial t} + \frac{\partial(\rho_M \alpha_M u_M)}{\partial x} = \dot{m}_B, \tag{17}$$

- gas momentum equation:

$$\frac{\partial(\rho_G \alpha_G u_G)}{\partial t} + \frac{\partial(\rho_G \alpha_G u_G^2)}{\partial x} = -\alpha_G \frac{\partial p}{\partial x} + \rho_G \alpha_G g \sin\beta + F_{wG} + F_i, \tag{18}$$

- mixture momentum equation:

$$\frac{\partial(\rho_M \alpha_M u_M)}{\partial t} + \frac{\partial(\rho_M \alpha_M u_M^2)}{\partial x} = -\alpha_M \frac{\partial p}{\partial x} - \rho_M \alpha_M g \frac{\partial h}{\partial x} \cos\beta + \rho_M \alpha_M g \sin\beta + F_{wL} - F_i, \tag{19}$$

where F_{wG} and F_{wL}, indicate respectively the forces exerted by the pipe walls on the gas and liquid-mixture phases, F_i is the interfacial force, p is the gas–liquid interface pressure, h is the height of the mixture layer, x and t represent the spatial and time coordinate respectively, the pipe incli-

nation is β, and the acceleration due to gravity is g. Variables with subscript M relate to the gas–liquid mixture, and it is worth remarking that, when no gas bubbles are present ($\alpha_B = 0$), the equations reduce to those for a pure liquid phase.

It has to be remarked that in deriving Eq. (19) an additional term containing the derivative of the drift velocity u_s is obtained. However, an order of magnitude analysis carried out by Bonizzi (2003) showed that the term is negligible due to the large density ratio between the gas and the liquid; hence it is dropped from that equation. Once again, this assumption is not essential to the model and the term could, if necessary, be retained in the equation.

When compared to the standard two-fluid model, the gas and liquid continuity equations ((16) and (17) respectively) possess a source term on the right hand side, denoted by $\dot{m}_B$, accounting for the mass exchange occurring at the front and tail of each slug. It should be noted that the momentum transfer due to the mass exchange has been neglected in the momentum equations since normally being much lighter, the gas carries negligible momentum compared to the liquid. A scalar-transport equation for the conservation of mass of the gas bubbles entrained within the liquid slug can be formulated from mass conservation considerations as:

$$\frac{\partial(\rho_G \alpha_B)}{\partial t} + \frac{\partial(\rho_G \alpha_B u_B)}{\partial x} = \dot{m}_B. \tag{20}$$

This equation serves to determine α_B as a function of x and t. In Eq. (20), the diffusion of bubbles in the axial direction is neglected, and the distribution of bubbles across the pipe cross-sectional area is assumed to be uniform.

Eqs. (16)–(20) are solved for the following primitive variables: the mixture velocity u_M, the gas velocity u_G, the pressure p, the gas fraction α_G and the slug voidage α_B. All other quantities can be expressed as function of these.

3. Model closure

Closure models are required for the wall-friction and inter-phase shear forces F_{wL}, F_{wG}, and F_i, the bubble velocity u_B, and the mass transfer between gas and liquid $\dot{m}_B$ both at the slug front and at its tail.

3.1. Shear forces

The inter-phase and gas-wall shear forces are expressed as in the existing model (Issa and Kempf, 2003) by:

$$F_i = \frac{-\tau_i S_i}{A} \tag{21}$$

and

$$F_{wG} = \frac{-\tau_{wG} S_G}{A}, \tag{22}$$

respectively. In the above equations, A is the pipe cross-sectional area, S_i and S_G designate the interfacial width and the gas wetted perimeter respectively, as shown in Fig. 2. The inter-phase and gas-wall shear stresses τ_i and τ_{wG} are commonly related to the dynamic pressure by:

$$\tau_i = \tfrac{1}{2} f_i \rho_G |u_G - u_L|(u_G - u_L) \tag{23}$$

and

$$\tau_{wG} = \tfrac{1}{2} f_G \rho_G |u_G| u_G, \tag{24}$$

respectively. The friction factors are based on the widely used model of Taitel and Dukler (1976). The expression for the gas-wall friction factor is:

$$f_G = C_G Re_G^{-n_G}, \tag{25}$$

where the Reynolds number is defined as:

$$Re_G = \frac{D_G u_G \rho_G}{\mu_G}. \tag{26}$$

The hydraulic diameter D_G is defined as:

$$D_G = \frac{4A_G}{(S_i + S_G)}. \tag{27}$$

The coefficients C_G and n_G respectively have values of 0.046 and 0.25 if the flow is turbulent ($Re_G > 2100$), or 16 and 1 if the flow is laminar ($Re_G \leqslant 2100$). The interfacial friction factor is expressed as:

$$f_i = C_i Re_i^{-n_i}, \tag{28}$$

where Re_i is defined as:

$$Re_i = \frac{D_G u_{rel} \rho_G}{\mu_G}. \tag{29}$$

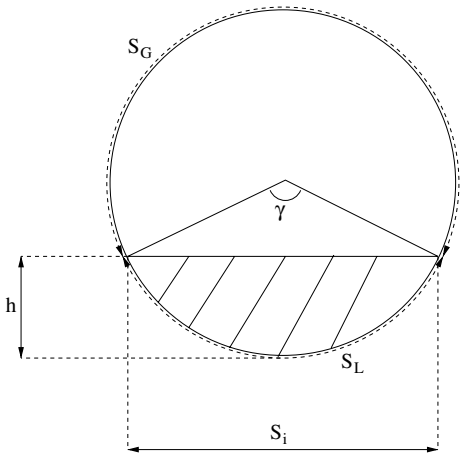

Fig. 2. Pipe cross-sectional area and relevant wetted properties for a two-phase stratified flow.

The velocity u_{rel} represents the gas–liquid slip velocity ($u_{\mathrm{rel}} = u_{\mathrm{G}} - u_{\mathrm{L}}$), while C_{i} and n_{i} have the same expressions as those for the gas friction factor.

The liquid-wall (or mixture-wall within an aerated slug) shear force is expressed as:

$$F_{\mathrm{wL}} = \frac{-\tau_{\mathrm{wL}} S_{\mathrm{L}}}{A}, \tag{30}$$

where the shear stress is given as follows:

$$\tau_{\mathrm{wL}} = \tfrac{1}{2} f_{\mathrm{d}} \rho_{\mathrm{L}} |u_{\mathrm{M}}| u_{\mathrm{M}}. \tag{31}$$

In the above equation, f_{d} is an *effective* friction factor that takes into account the correction proposed by Malnes (1982), who noticed an increase in friction in slugs containing gas bubbles. Thus, the friction factor for dispersed gas–liquid flow f_{d} is related to that for the pure liquid phase flowing alone in the pipe f_{L} by the following equation:

$$f_{\mathrm{d}} = \phi_{\mathrm{d}} f_{\mathrm{L}}, \tag{32}$$

where $\phi_{\mathrm{d}} = 1$ along the whole flow domain, except within an aerated slug, where the correction factor of Malnes (1982) is used:

$$\phi_{\mathrm{d}} = \frac{1}{1 - \alpha_{\mathrm{B}}} \left[1 + 15.3 \frac{\alpha_{\mathrm{B}}}{\sqrt{(1 - \alpha_{\mathrm{B}})}} \frac{u_{\infty}}{u_{\mathrm{M}}} \right]. \tag{33}$$

Here, u_{∞} is the terminal velocity of an isolated bubble rising in an infinite medium, given by:

$$u_{\infty} = 1.18 \left[\frac{g\sigma(\rho_{\mathrm{L}} - \rho_{\mathrm{G}})}{\rho_{\mathrm{L}}^2} \right]^{0.25}, \tag{34}$$

and σ is the gas–liquid surface tension. It should be emphasised here that the present model is not predicated on the use of the Malnes correlation given by Eq. (33); other models to account for the increase in friction when bubbles are present can be used equally well.

The correlation used for calculating the liquid-wall friction factor f_{L}, is that of Hand (1991), and Spedding and Hand (1997). It is expressed as:

$$f_{\mathrm{L}} = \frac{24}{Re_{\mathrm{L}}^{s}}, \tag{35}$$

if the liquid flow is laminar. This is determined by the liquid Reynolds number Re_{L}, thus:

$$Re_{\mathrm{L}} = \frac{\rho_{\mathrm{L}} D_{\mathrm{L}} u_{\mathrm{L}}}{\mu_{\mathrm{L}}} \leqslant 2100, \tag{36}$$

where the hydraulic diameter D_{L} is given by:

$$D_{\mathrm{L}} = \frac{4A_{\mathrm{L}}}{S_{\mathrm{L}}}. \tag{37}$$

If the liquid flow is turbulent ($Re_{\mathrm{L}} > 2100$), then

$$f_{\mathrm{L}} = 0.0262 (\alpha_{\mathrm{L}} Re_{\mathrm{L}}^{s})^{-0.139}. \tag{38}$$

In Eqs. (35) and (38), the liquid Reynolds number Re^s_L is based on the liquid superficial velocity:

$$Re^s_L = \frac{\rho_L U_L D}{\mu_L}. \tag{39}$$

3.2. Bubble velocity

The bubble velocity in Eq. (20) needs to be specified and a closure model is required for that purpose; it is here where a drift-flux type relationship is introduced. In reality, the dispersed bubble distribution across the pipe section may not be uniform (tending to concentrate at the top) and this depends on the flow rate. Also, the bubbles are unlikely to be of uniform size. In a one-dimensional model these effects are subsumed in the averaging process but can be accounted for approximately: the first by a correction factor which modifies an assumed uniform profile, and the second by the solution of several transport equation like (20) for a range of bubble diameters. However, such model refinements are not implemented here as the phenomena are considered to be of second order importance and are hence ignored for the purpose of this article.

The dynamics of the entrained bubbles are naturally governed by the usual laws of motion. However, in this work it is assumed that the inertial forces are negligible (this can easily be established by an order of magnitude analysis) and that the bubbles attain a state of equilibrium instantaneously. Thus, a local balance between the forces acting on the bubbles (Bonizzi et al., 2001) is assumed to exist at all times. The most significant forces encountered by a bubble moving in a liquid stream may reasonably be assumed to be the pressure (F_p) and drag (F_D) forces (see Fig. 3). Assuming steady motion of the bubble, the balance of these forces may be written as:

$$\frac{1}{2} u_s^2 A_B \rho_L C_D = -\frac{dp}{dx} V_B, \tag{40}$$

where A_B and V_B are the cross-sectional area and volume of the gas bubble respectively. Rearrangement of this equation and assuming a spherical bubble of diameter d_B gives:

$$u_s = -\sqrt{\frac{-4 d_B (dp/dx)}{3 C_D \rho_L}}. \tag{41}$$

From Eqs. (12) and (41), the bubble velocity can finally be obtained as:

$$u_B = u_M - \sqrt{\frac{-4 d_B (dp/dx)}{3 C_D \rho_L}}. \tag{42}$$

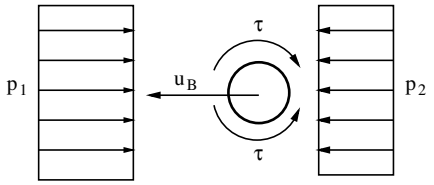

Fig. 3. Forces acting on a single bubble.

In this equation, the pressure and the mixture velocity are two of the primitive variables that are determined as an outcome of the solution of the discretised transport equations (16)–(20). Within the body of the slug the pressure drops from the slug tail to its front (hence implying a negative pressure gradient); this means that the bubbles will travel more slowly than the liquid through the slug (in a reference frame attached to the slug body). This indeed corresponds to experimental observations.

Two other quantities appearing in Eq. (42) need specification, these are the drag coefficient on the bubble C_D and the bubble diameter d_B. Following the experimental findings of Andreussi et al. (1993), the diameter of the entrained bubbles may be assumed to be constant and equal to 1 mm. This value is likely to be valid only for that particular experiment, but in the absence of better information, it is utilised here. This assumption can be readily removed when better correlations for the entrained bubble diameter become available.

The drag coefficient C_D is calculated from the correlation of Tomiyama et al. (1995), who proposed a modification for the drag coefficient for a bubble due to the presence of a swarm of bubbles. Their correlation is expressed as:

$$C_D = \frac{C_{DT}}{\sqrt{\alpha_{Ls}}}, \tag{43}$$

where

$$C_{DT} = \max\left[\frac{24}{Re_B}\left(1 + 0.15Re_B^{0.687}\right), \frac{8}{3}\frac{Eo}{Eo+4}\right]. \tag{44}$$

In Eq. (44) Re_B and Eo represent the bubble Reynolds and Eötvös numbers. The former is given by:

$$Re_B = \frac{\rho_L d_B |u_M - u_B|}{\mu_L}, \tag{45}$$

and the latter by:

$$Eo = \frac{g(\rho_L - \rho_G)d_B^2}{\sigma}. \tag{46}$$

3.3. Mass exchange rates

The shedding rate of dispersed bubbles at the slug tail is obtained by assuming that all the bubbles arriving at the tail leave the slug and enter the large gas bubble behind it. Hence:

$$\dot{M}_B = \rho_G A(u_b - u_B)\alpha_B, \tag{47}$$

where u_b represents the local velocity at which the tail of the slug propagates (see Fig. 4) and whose value is determined as explained later. The entrainment rate at the slug front must however be obtained from an independent correlation. Not many such correlations are available in the literature, and only three could be found. One was proposed by Nydal and Andreussi (1991), who investigated, at atmospheric conditions, air–water aerated slugs advancing over a slow moving liquid layer in a nearly horizontal pipe. Their correlation is expressed by:

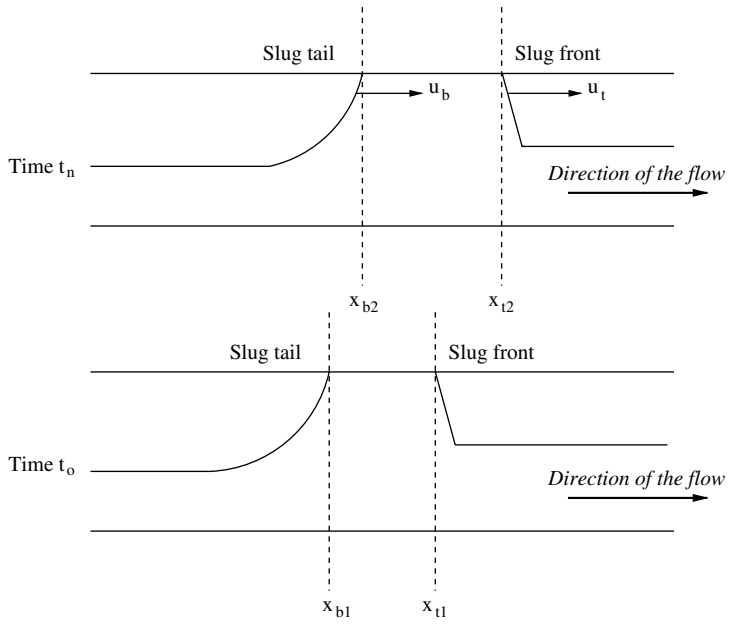

Fig. 4. Displacement of front and tail of the slug as it travels along the pipe.

$$\dot{M}_{\mathrm{B}} = \rho_{\mathrm{G}} A \left(0.076 \frac{S_{\mathrm{i}}}{D} (u_{\mathrm{t}} - u_{\mathrm{Lf}}) - 0.15 \right), \tag{48}$$

where u_{t} represents the velocity of propagation of the front of the slug (see Fig. 4), u_{Lf} the velocity of the liquid in the film region, and S_{i} the gas–liquid interfacial width in the film. The second correlation is due to Manolis (1995):

$$\dot{M}_{\mathrm{B}} = 1.871 \rho_{\mathrm{G}} A S_{\mathrm{i}} [(u_{\mathrm{t}} - u_{\mathrm{Lf}}) - 2.126]. \tag{49}$$

The latter is derived from observations of slug front behaviour in air–water pipe flow at atmospheric conditions in a push-in experiment, in a 1° upward inclined pipe.

Since the entrainment is a consequence of the pick-up rate, due to the entrance of the liquid film into the liquid slug, one could associate this phenomenon with the air carry-under and bubble dispersion process associated with a plunging jet (Bonetto and Lahey, 1993). As a limiting case of plunging jet flow in horizontal configurations, the hydraulic jump (Chanson, 1996) provides another possible model, to be compared against the purely empirical ones given by Eqs. (48) and (49). Among the many available correlations for a hydraulic jump, the one recommended by Chanson (1996) is used here since it is reportedly to be the most widely used in engineering practice due to its superior performance. It is expressed as:

$$\dot{M}_{\mathrm{B}} = \rho_{\mathrm{G}} A_{\mathrm{Lf}} (u_{\mathrm{t}} - u_{\mathrm{Lf}}) \zeta (Fr - 1)^{\varepsilon}, \tag{50}$$

where the Froude number is based on the relative velocity between the slug front and liquid film, $u_{\mathrm{t}} - u_{\mathrm{Lf}}$, which corresponds to the velocity of the liquid jet entering the liquid slug in a relative frame moving at the slug front velocity. The expression for the Froude number is:

$$Fr = \frac{u_t - u_{Lf}}{\sqrt{gA_{Lf}/S_i}}, \tag{51}$$

where A_{Lf} represents the area occupied by the liquid in the film. The coefficients ζ and ε are functions of the Froude number (Rajaratnam, 1967; Wisner, 1965) and their values are:

$$\zeta = 0.018, \quad \varepsilon = 1.245 \qquad \text{if } 2.5 < Fr < 7, \tag{52}$$

or

$$\zeta = 0.014, \quad \varepsilon = 1.4 \qquad \text{if } 7 < Fr < 30. \tag{53}$$

The onset of entrainment depends on the velocity difference between the translational velocity of the slug front, and the liquid film velocity (Andreussi and Bendiksen, 1989; Nydal and Andreussi, 1991; Manolis, 1995). The onset will occur when:

$$u_t - u_{Lf} > 2.126 \text{ (m/s)}, \tag{54}$$

in Eq. (49),

$$u_t - u_{Lf} > 1.974\frac{D}{S_i} \text{ (m/s)}, \tag{55}$$

in Eq. (48), or

$$u_t - u_{Lf} > \sqrt{g\frac{A_{Lf}}{S_i}} \text{ (m/s)}, \tag{56}$$

in Eq. (50). All of the above alternative correlations were implemented and tested against experimental data in the work presented herein; the results are summarised later.

It should be stressed that, despite the clear evidence of the strong effect of surface tension and liquid viscosity on the slug voidage (Bendiksen et al., 1996), none of the above correlations takes into account the physical properties of the liquid. This deficiency will need further investigation in future.

The mass transfer rate $\dot{m}_B$ in Eq. (20) is per unit volume. The net mass flow rate in Eqs. (47)–(50) is therefore related to $\dot{m}_B$ by:

$$\dot{M}_B = \int \dot{m}_B A \, dx. \tag{57}$$

3.4. Film and slug front/tail velocities

In order to predict both onset and rate of entrainment, the relative velocity between the slug front and the film has to be calculated. Also, to compute the bubble shedding rate, the slug tail velocity has to be found. Furthermore, the position of the slug front and tail need to be determined in order to introduce the mass transfer at those locations. All of this can be achieved by continually monitoring the slugs as they proceed along the pipe (Fig. 5).

Identifying the slug fronts and tails is easy: these are the locations where the gas phase fraction vanishes. The position of the liquid film, where the value of the film velocity u_{Lf} is needed, is assumed to be where the liquid height h changes slope (see Fig. 5).

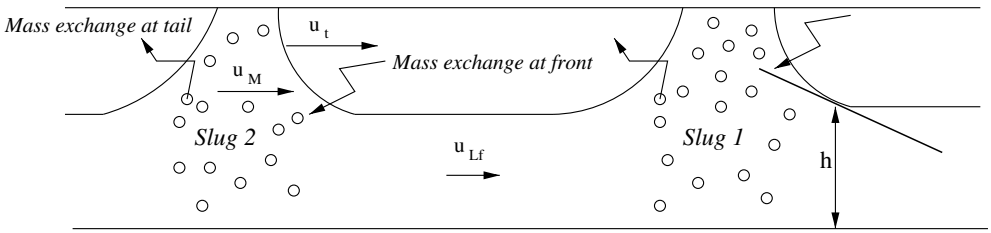

Fig. 5. Quantities needed to calculate the entrainment rate.

In order to determine the slug front and tail velocities, u_t and u_b (the former required by Eqs. (48)–(50), the latter by Eq. (47)) two methods have been tried, both of which give similar results. In the first, a simple but empirical technique is implemented based on the widely accepted correlation of Bendiksen (1984) which relates the slug velocity to that of the mixture. It is assumed herein that the front and tail of a slug travel at the same velocity. Hence, both slug velocities are based on the following equation:

$$u_b = C_0 u_M + u_d \tag{58}$$

with the distribution parameter C_0 and drift velocity u_d being 1.2 and 0, or 1.05 and $0.54\sqrt{gD}$ depending on whether the mixture Froude number ($Fr_M = U_M/(\sqrt{gD})$) is greater or smaller than the critical value of 3.5 respectively. For a horizontal pipe with internal diameter of 0.078 mm, the Bendiksen correlation reduces to:

$$u_b = 1.2 u_M \tag{59}$$

provided that the mixture velocity is greater than 3.06 m/s.

The alternative method for determining these velocities is to continually track the movements of each slug front and tail in time and then calculate the velocities simply from the displacement of these points over successive time steps in the numerical integration. Referring to Fig. 4, the numerically computed slug velocities may be expressed as:

$$u_t = \frac{x_{t2} - x_{t1}}{t_n - t_0}, \tag{60}$$

for the front, and

$$u_b = \frac{x_{b2} - x_{b1}}{t_n - t_0}, \tag{61}$$

for the tail, where $t_n - t_0$ denotes the time interval for that integration step. Although this procedure is straight forward, it does entail tedious bookkeeping.

Both of the above approaches to the estimation of the instantaneous slug front/tail velocity were tried in the present computations. It was found that although the numerically computed slug velocity was in general different from the Bendiksen correlation (see subsequent section for comparison), the values obtained were fairly close, especially when the slugs attained an equilibrium state. Moreover, when used in the mass transfer rate expressions (Eqs. (47)–(50)), these values gave few significant differences. Therefore, for the sake of expediency, the Bendiksen approximation was employed in the main.

3.5. Summary

The model for gas entrainment in horizontal or nearly horizontal two-phase slug flow consists of equations for the conservation of mass and momentum (16)–(19) for the gas and liquid–gas mixture phases, and of an equation for the calculation of the bubble voidage in the liquid slug (20). The model is closed by an equation for the slip velocity of the bubbles (41), an equation for the shedding rate of bubbles at the slug tail (47), by one of three equations (48), (49), or (50) for bubble entrainment rate at the slug front, and by Eq. (58) for the computation of the instantaneous slug front and tail velocities.

4. Characteristics analysis

Although gas compressibility effects are taken into account in the present model, the analysis of the compressible form of the model equations is too complex to present here. In any event, the hyperbolic nature of the system should emerge whether the fluids are compressible or not, and the outcome would be little affected by fluid compressibility (two more characteristics arise in the latter case). Hence the analysis presented below pertains to incompressible fluids. Also for brevity, the analysis is carried out for a horizontal pipe ($\beta = 0$).

The set of Eqs. (16)–(20) represents a system of first order partial differential equations that can be written in a more compact form as:

$$A\frac{\partial \Phi}{\partial t} + B\frac{\partial \Phi}{\partial x} = C, \tag{62}$$

where A and B are coefficient matrices, Φ is the solution vector here corresponding to

$$\Phi = [\alpha_G, \alpha_B, u_G, u_M, p]^T, \tag{63}$$

and C is a vector containing all the algebraic terms. The initial value problem under consideration is to find a solution of system (62) in some region:

$$a \leqslant x \leqslant b, \quad t \geqslant 0, \tag{64}$$

subject to the initial condition:

$$\Phi(t = 0, x) = G(x), \tag{65}$$

and values of Φ or its derivatives defined on the boundaries $x = a$ and $x = b$. The system (62) is defined to be well-posed (or hyperbolic) when the equations with appropriate boundary conditions and initial values admit a unique solution and this solution depends continuously on the initial data and boundary conditions. The mathematical character of a set of partial differential equations is provided by the solution of the *eigenvalue system* (Hirsch, 1988):

$$\det[B - \lambda A] = 0. \tag{66}$$

A necessary condition for the system to be well-posed, is that the roots (that physically represent the characteristics of the system) of Eq. (66) are all real. The characteristics represent the velocities at which the information travels through the domain; in other words the information propagates in as many directions as there are eigenvalues associated with the set of equations.

For the set of Eqs. (16)–(20), the matrices A and B are:

$$A = \begin{bmatrix} 1 & 0 & 0 & 0 & 0 \\ -1 & 0 & 0 & 0 & -\alpha_M \Delta\rho \\ 0 & \alpha_G & 0 & 0 & 0 \\ 0 & 0 & \alpha_M & 0 & 0 \\ 0 & 0 & 0 & 0 & 1 \end{bmatrix} \tag{67}$$

and

$$B = \begin{bmatrix} u_G & \alpha_G & 0 & 0 & 0 \\ -u_M & 0 & \alpha_M & 0 & -\alpha_M u_M \Delta\rho \\ 0 & \alpha_G u_G & 0 & \alpha_G/\rho_G & 0 \\ \frac{-\pi\alpha_M g D}{4\sin(\gamma/2)} & 0 & \alpha_M u_M & \alpha_M/\rho_M & 0 \\ 0 & 0 & 0 & 0 & u_B \end{bmatrix}, \tag{68}$$

where $\Delta\rho \equiv (\rho_L - \rho_G)/\rho_M$ and γ denotes the liquid stratification angle, as indicated in Fig. 2. Substitution of the matrices given by (67) and (68) into Eq. (66) gives a cubic algebraic equation for the eigenvalues λ, with three solutions that represent three characteristics. The first solution:

$$\lambda_1 = u_B \tag{69}$$

corresponds to the bubble velocity. The other two are:

$$\lambda_{2,3} = \frac{(a u_G + b u_M) \pm \sqrt{\frac{(a+b)\alpha_G(1-\alpha_G)\rho_M \pi g D}{4\sin(\gamma/2)} - ab(u_G - u_M)^2}}{a+b}, \tag{70}$$

where $a \equiv \rho_G(1-\alpha_G)$ and $b \equiv \rho_M \alpha_G$; these are identical to the characteristics arising from the unaerated two-fluid model equations for stratified flow (see Banerjee and Chan, 1980; Chun and Sung, 1996). The last two characteristics are real (and also positive) when:

$$(u_G - u_M)^2 \leqslant \left(\frac{\alpha_M}{\rho_M} + \frac{\alpha_G}{\rho_G}\right) \frac{\pi D}{4\sin(\gamma/2)} g\rho_M. \tag{71}$$

This represents the condition for which the system of equations becomes hyperbolic and hence well-posed. Meaningful solutions to the model only exist therefore when this condition is met (see Issa and Kempf, 2003).

When compressibility of the gas phase is taken into account as is the case with the model actually used here, two more characteristics arise corresponding to the propagation of pressure waves (see Bonizzi, 2003). These are given by:

$$\lambda_{4,5} = \pm c, \tag{72}$$

where c is the speed of sound. Thus, there are five characteristics in all, dictating the number of boundary conditions that must be imposed. Since four of the characteristics run in the positive direction, four boundary conditions are needed at inlet and one at outlet.

5. Numerical implementation

The model was implemented in a computer code called TRIOMPH (Issa and Abrishami, 1986; Issa and Kempf, 2003), into which two additional modules were incorporated. The first is used to monitor the position of each slug travelling in the pipe in order to identify the computational cells where mass is exchanged between the gas and mixture phases. The rates of entrainment at the slug front and tail are subsequently calculated. The purpose of the second module is to solve the scalar-transport equation for the average bubble concentration in the liquid slug (Eq. (20)). All entrainment rate relationships presented above (i.e. Eq. (48) by Nydal and Andreussi (1991), Eq. (49) by Manolis (1995), and Eq. (50) from the hydraulic jump theory of Rajaratnam (1967) and Wisner (1965)) were implemented and compared. Once the volume fraction of bubbles entrained in the liquid is obtained from Eq. (20), the mixture density ρ_M is determined (from Eq. (15)), and this in turn enters into the equations for the conservation of momentum and mass.

The equations solved by the model are (16)–(20), and therefore the solution vector consists of the following variables (see Eq. (63)): gas phase fraction, slug voidage, gas and liquid centre of mass velocity, and interfacial pressure. The discretisation method used is the same as that described by Issa and Kempf (2003): the model equations are integrated using a finite-volume formulation, and discretised using a first order fully implicit scheme in time, and a first order upwind scheme in space. Fig. 6 shows the staggered grid arrangement for the one-dimensional domain, with control volumes given for velocity and pressure cells. In the figure, symbols e and w denote the boundaries of the volumes that are centred on node p.

The finite-volume formulation of the continuity equation, integrated between the times t_0 and $t_n = t_0 + \Delta t$, is given, for either gas or liquid, by:

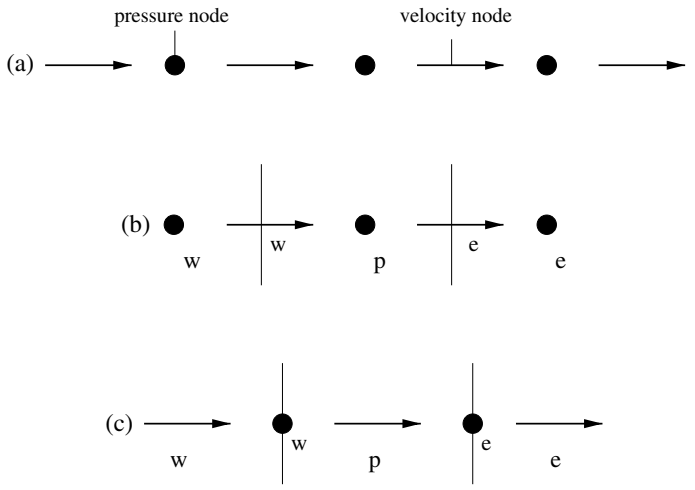

Fig. 6. Staggered grid arrangement: (a) staggered mesh, (b) scalar control volume, and (c) velocity control volume.

$$\left(\frac{\Delta x}{\Delta t}\rho_{\mathrm{p}}^{n}+\max[\rho_{\mathrm{w}}^{n}u_{\mathrm{w}}^{n},0]+\max[-\rho_{\mathrm{e}}^{n}u_{\mathrm{e}}^{n},0]+(\rho_{\mathrm{e}}^{n}u_{\mathrm{e}}^{n}-\rho_{\mathrm{w}}^{n}u_{\mathrm{w}}^{n})\right)\alpha_{\mathrm{p}}^{n}$$
$$=\max[\rho_{\mathrm{w}}^{n}u_{\mathrm{w}}^{n},0]\alpha_{\mathrm{w}}^{n}+\max[-\rho_{\mathrm{e}}^{n}u_{\mathrm{e}}^{n},0]\alpha_{\mathrm{e}}^{n}+\frac{\Delta x}{\Delta t}\rho_{\mathrm{p}}^{0}\alpha_{\mathrm{p}}^{0}, \tag{73}$$

that can be written in a more compact form as:

$$a_{\mathrm{p}}\alpha_{\mathrm{p}}^{n}=a_{\mathrm{w}}^{n}\alpha_{\mathrm{w}}^{n}+a_{\mathrm{e}}^{n}\alpha_{\mathrm{e}}^{n}+S_{\alpha}, \tag{74}$$

where a_{e}, a_{w}, and a_{p} are finite difference coefficients representing the convective fluxes and S_{α} containing the rest of the terms. The discretised momentum equation is as follows:

$$\left(\frac{\Delta x}{\Delta t}\rho_{\mathrm{p}}^{n}\alpha_{\mathrm{p}}^{n}+\max[-\rho_{\mathrm{e}}^{n}\alpha_{\mathrm{e}}^{n}u_{\mathrm{e}}^{n},0]+\max[\rho_{\mathrm{w}}^{n}\alpha_{\mathrm{w}}^{n}u_{\mathrm{w}}^{n},0]+\left(\rho_{\mathrm{e}}^{n}\alpha_{\mathrm{e}}^{n}u_{\mathrm{e}}^{n}-\rho_{\mathrm{w}}^{n}\alpha_{\mathrm{w}}^{n}u_{\mathrm{w}}^{n}\right)\right)u_{\mathrm{p}}^{n}$$
$$=\max[\rho_{\mathrm{w}}^{n}\alpha_{\mathrm{w}}^{n}u_{\mathrm{w}}^{n},0]u_{\mathrm{w}}^{n}+\max[-\rho_{\mathrm{e}}^{n}\alpha_{\mathrm{e}}^{n}u_{\mathrm{e}}^{n},0]u_{\mathrm{e}}^{n}-\alpha_{\mathrm{p}}^{n}(p_{\mathrm{e}}^{n}-p_{\mathrm{w}}^{n})+\frac{\Delta x}{\Delta t}\rho_{\mathrm{p}}^{0}\alpha_{\mathrm{p}}^{0}u_{\mathrm{p}}^{0}+S_{u}, \tag{75}$$

where S_u stands for the whole of the source terms in Eqs. (18) and (19). Eq. (75) can be written in a more compact form using the operator H that stands for the finite-volume representation of the spatial convective fluxes, as:

$$\frac{\Delta x}{\Delta t}\left(\rho_{\mathrm{p}}^{n}\alpha_{\mathrm{p}}^{n}u_{\mathrm{p}}^{n}-\rho_{\mathrm{p}}^{0}\alpha_{\mathrm{p}}^{0}u_{\mathrm{p}}^{0}\right)=H_{u}(u_{\mathrm{p}}^{n})-\alpha_{\mathrm{p}}^{n}(p_{\mathrm{e}}^{n}-p_{\mathrm{w}}^{n})+S_{u}. \tag{76}$$

An overall continuity equation can now be obtained by combining the two continuity equations for the gas and liquid phases (16) and (17), each weighted by an appropriate reference density, to give:

$$\frac{\Delta x}{\Delta t}\left(\frac{1}{\rho_{\mathrm{M}}^{\mathrm{ref}}}\left(\alpha_{\mathrm{M,p}}^{n}\rho_{\mathrm{M,p}}^{n}-\alpha_{\mathrm{M,p}}^{0}\rho_{\mathrm{M,p}}^{0}\right)+\frac{1}{\rho_{\mathrm{G}}^{\mathrm{ref}}}\left(\alpha_{\mathrm{G,p}}^{n}\rho_{\mathrm{G,p}}^{n}-\alpha_{\mathrm{G,p}}^{0}\rho_{\mathrm{G,p}}^{0}\right)\right)$$
$$+\frac{1}{\rho_{\mathrm{M}}^{\mathrm{ref}}}\left(\alpha_{\mathrm{M,e}}^{n}\rho_{\mathrm{M,e}}^{n}u_{\mathrm{M,e}}^{n}-\alpha_{\mathrm{M,w}}^{n}\rho_{\mathrm{M,w}}^{n}u_{\mathrm{M,w}}^{n}\right)+\frac{1}{\rho_{\mathrm{G}}^{\mathrm{ref}}}\left(\alpha_{\mathrm{G,e}}^{n}\rho_{\mathrm{G,e}}^{n}u_{\mathrm{G,e}}^{n}-\alpha_{\mathrm{G,w}}^{n}\rho_{\mathrm{G,w}}^{n}u_{\mathrm{G,w}}^{n}\right). \tag{77}$$

If the velocities, expressed as in Eq. (76) are now substituted (for details see Bonizzi, 2003) into the overall continuity equation (77), an equation for the pressure is obtained in the form:

$$a_{\mathrm{p}}^{n}p_{\mathrm{p}}^{n}=a_{\mathrm{w}}^{n}p_{\mathrm{w}}^{n}+a_{\mathrm{e}}^{n}p_{\mathrm{e}}^{n}+S_{\mathrm{p}}. \tag{78}$$

A sequential iterative method is used to solve the system of discretised equations at each time step. The equations solved in the sequence are as follows:

- mixture momentum equation (19),
- gas momentum equation (18),
- pressure equation (78),
- gas continuity equation (16),
- gas bubble equation (20).

Each of the sets of Eqs. (19), (18), (78), (16) and (20) constitutes a tri-diagonal matrix system which can be solved directly using coefficients based on old iteration values. The iteration loop is

executed until the residuals in each equation become smaller than a fixed tolerance. Once convergence is achieved for the given step, a new time increment is calculated based on the following dimensionless number:

$$\frac{u^n_{\mathrm{G,max}}\,\Delta t}{\Delta x} = C, \tag{79}$$

where the constant C in Eq. (79) is typically set at 0.5.

The boundary conditions imposed must reflect both the physics and the mathematical character of the governing equations (see Section 4). Here, five quantities (corresponding to the five characteristics of the equations) must be specified, four at inlet and one at outlet (dictated by the directions of the characteristics). At the inlet of the pipe the total liquid hold-up, the dispersed bubbles voidage (taken to be zero) and the superficial velocities of the gas and liquid are specified and assumed to remain steady at those values. At the outlet, the pressure is prescribed. The initial conditions correspond to stratified flow with uniform velocity, phase fractions, and pressure fields.

Liquid slugs generate automatically and are captured in the same way as in two-phase flow using the "slug capturing" methodology (Issa and Woodburn, 1998; Issa and Kempf, 2003). The method, allows liquid slugs to be captured as a mechanistic and automatic outcome of the growth of hydrodynamic instabilities in an Eulerian frame. In order to capture the natural growth of disturbances at the gas–liquid interface, the numerical resolution must be high. In order to achieve such accuracy with the currently used first order spatial and temporal discretisation schemes, very fine computational grids were utilised (typically $\Delta x/D \approx 0.4$ was found to be sufficient). Systematic checks were carried to verify that all the results are independent of the grid, as Fig. 7 demonstrates for a typical case of aerated slug flow. In the figure, various time-averaged slug characteristics at a particular location in the pipe (close to the outlet) obtained from different meshes are compared. The results show very little sensitivity to the mesh density thereby verifying their accuracy; this also indirectly indicates the well-posed nature of the model equations which otherwise would not have led to this convergence (see Issa and Kempf, 2003).

6. Results

Two different pipe geometries are chosen in order to validate the model. The first configuration is horizontal at atmospheric pressure, where hydrodynamic slugs generate. The second geometry is composed of a V-section (see Fig. 8), consisting of a downward and upward inclined sections (angle with respect to the horizontal $\beta \pm 1.5°$), where slugs form partly because of terrain-induced effects. It should be noted that the set of experimental data chosen for validation is independent of the closure relations used in the present model, thereby bolstering confidence in the validation exercise. But it should also be remarked that measurements in the literature show wide scatter in the data for slug characteristics, hence validation of the model ought to be made against a range of data sets originating from different sources. However, the set of measurements chosen here are claimed to be accurate, with error margins no larger than 5%. Another good reason for the present choice is the availability of detailed information on the boundary conditions which enables meaningful comparison between computations and experiment. Nonetheless, the validation

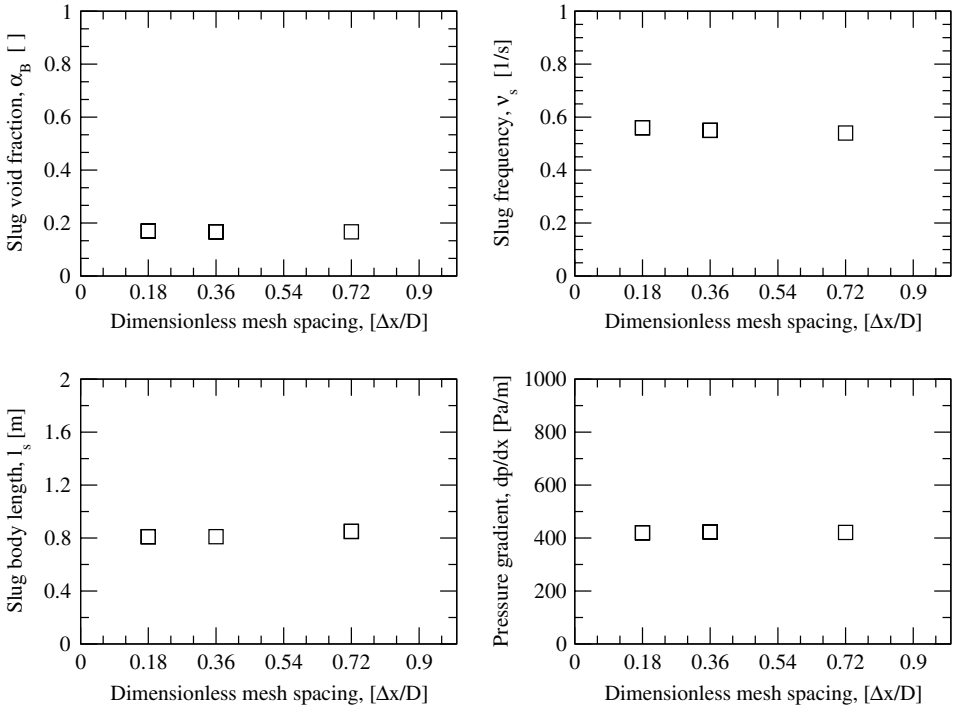

Fig. 7. Grid-dependence test for an aerated slug flow case.

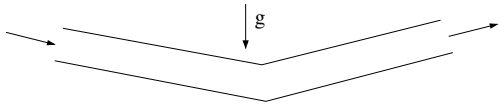

Fig. 8. V-section geometry.

presented herein cannot be treated as definitive until comparisons with other sets of data are carried out.

6.1. Horizontal pipe configuration

Calculations are made for air–water flow at atmospheric conditions in a horizontal pipe, 36 m long of internal diameter 0.078 m. The gas is treated as compressible, of constant dynamic viscosity of 1.77×10^{-5} Pa s. The gas–liquid surface tension is taken to be $\sigma = 0.07$ N/m. Standard boundary conditions are used to start the transient simulation (fixed outlet pressure corresponding to atmospheric value, constant superficial velocities and liquid hold-up at the pipe inlet). The initial hold-up, gas and liquid velocities are assumed to be uniform along the pipe corresponding to a stratified flow regime. The computational mesh is made up of 1250 cells. Four different flow rates ranging from low to intermediate mixture velocities are studied. Table 1 shows the gas, liquid, and mixture velocities for the four test cases. The slug characteristics for the cases

Table 1
Superficial and mixture velocities for horizontal slug flow test cases

Case	U_G (m/s)	U_L (m/s)	U_M (m/s)
RUN36	1.548	0.519	2.067
RUN40	1.945	0.751	2.696
RUN42	2.476	1.049	3.525
RUN25	3.463	0.737	4.2

listed in the table are provided by Manolis (1995), who studied this flow experimentally using conductivity probes with an error of ±1.5%.

Fig. 9 compares the experimental slug voidage α_B measured by Manolis, against the four empirical correlations described in the introduction. It can be seen that the correlations by Andreussi and Bendiksen (1989) and Abdul-Majeed (2000) (Eqs. (5) and (9) respectively) consistently under-predict the experimental data, while those by Malnes (1982) and Gregory et al. (1978) (Eqs. (3) and (1) respectively) over-predict them. Although it is quite evident from the figure that the empirical correlations do not compare well with the experimental data, they do exhibit the expected trend of increasing slug voidage with increasing mixture velocity.

The comparisons between the Manolis data (1995) and the present numerical predictions obtained using the rates of entrainment in Eqs. (48)–(50), are displayed in Fig. 10. The predicted values of slug voidage, plotted in the figure, are statistically averaged, as is done for all other slug characteristics that will be treated in this work. The predictions follow the experimental trend with increasing mixture velocities. From the figure it may be deduced that the experimental data are matched best when the hydraulic jump correlation (Eq. (50)) is used (discrepancy of 9.5%), although the Manolis equation (49) leads to reasonable results as well (with a discrepancy of 23%). The

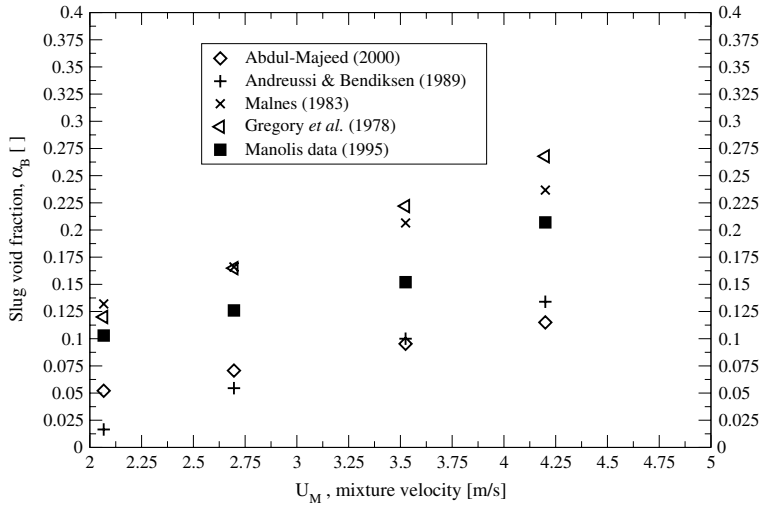

Fig. 9. Slug void fraction measurements by Manolis (1995) compared against some empirical correlation.

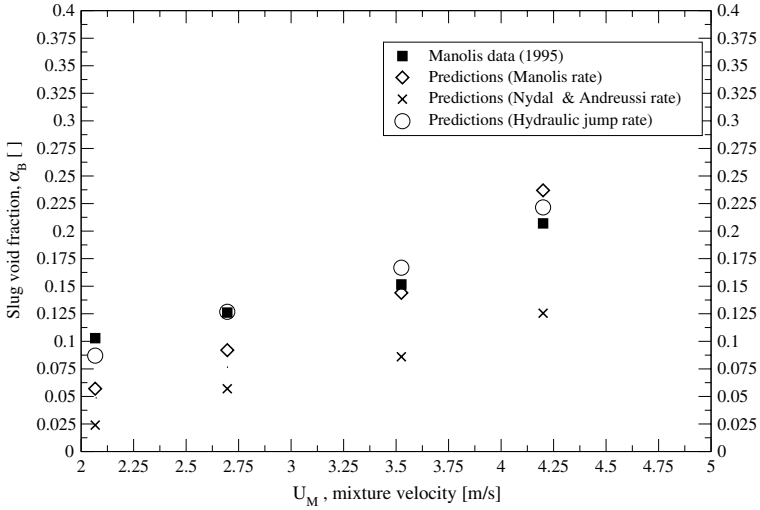

Fig. 10. Slug void fractions: comparison between measurements by Manolis (1995) and numerical predictions.

correlation of Nydal and Andreussi (1991) grossly under-predicts the measured slug voidage by nearly 55%.

Since both entrainment and shedding rates are based on the Bendiksen correlation, Eq. (58), for the slug front and tail velocities, it is of interest to evaluate the accuracy of this correlation against the numerically computed values that are outcome of the transient simulation itself, i.e. Eqs. (60) and (61). This comparison was made for each instant of time for a typical slug as it travelled along the pipe. First, in Fig. 11 the numerically computed slug velocity at location $L/D = 360$ (corresponding to the position of the experimental measurements), is evaluated against available ex-

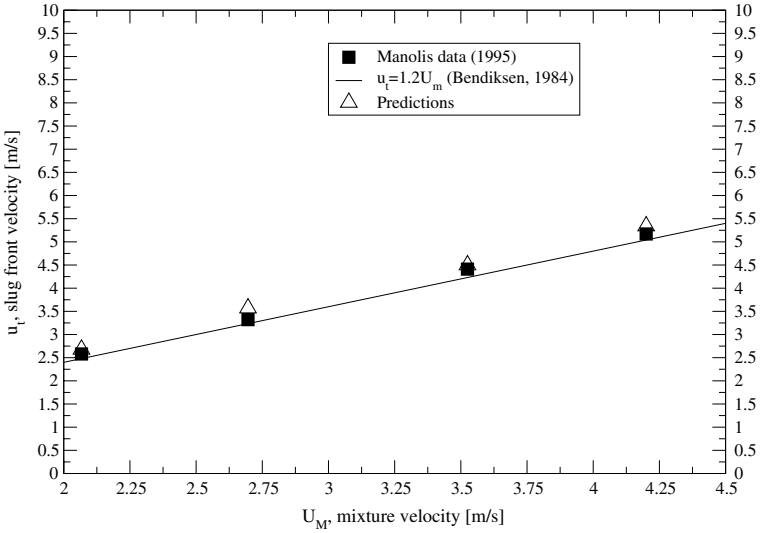

Fig. 11. Slug translational velocity: comparison between measurements by Manolis (1995) and numerical predictions.

perimental data; excellent agreement is found, with a discrepancy of about 4%. Next, in Fig. 12 the Bendiksen approximation is compared against the numerically computed slug front and tail velocities, for each of the four runs studied. The velocities are plotted as a function of distance along the pipe, i.e. as the slug front and tail pass through each particular location. The results are shown for one typical slug in each case as it initiates in the pipe (hence the differences in the plotted x-coordinate). Although Eq. (58) mostly under-predicts both numerical slug velocities during the transient period (the slug development region), the discrepancies become reasonably low in the "steady state" (or fully developed region, closer to the pipe exit) with maximum average errors of 15%. The effect of these discrepancies on the entrainment rates (where these velocities are used) is even smaller, hence justifying use of the Bendiksen correlation.

6.1.1. Bubble distribution along the liquid slug

Fig. 13 shows the gas void fraction distribution inside a slug for the case with the smallest mixture velocity ($U_M = 2.067$ m/s) when the hydraulic jump rate (Eq. (50)) is used. The other three runs

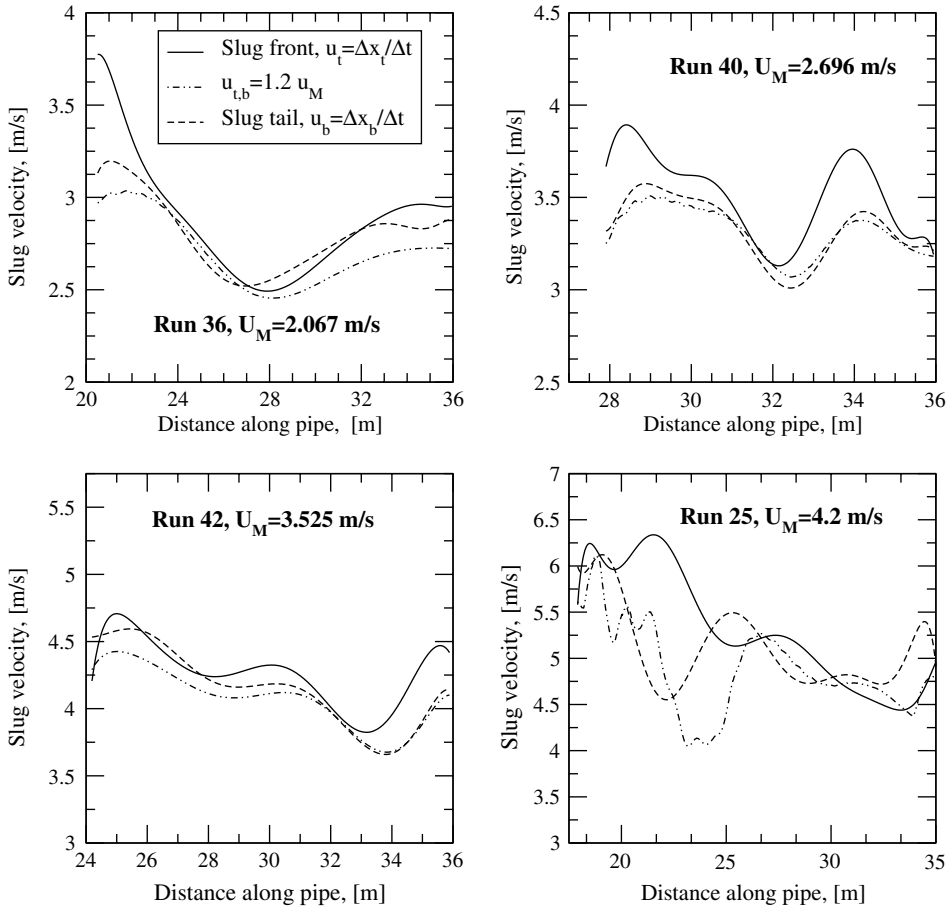

Fig. 12. Numerically computed slug tail and front velocity compared with Bendiksen empirical correlation (1984).

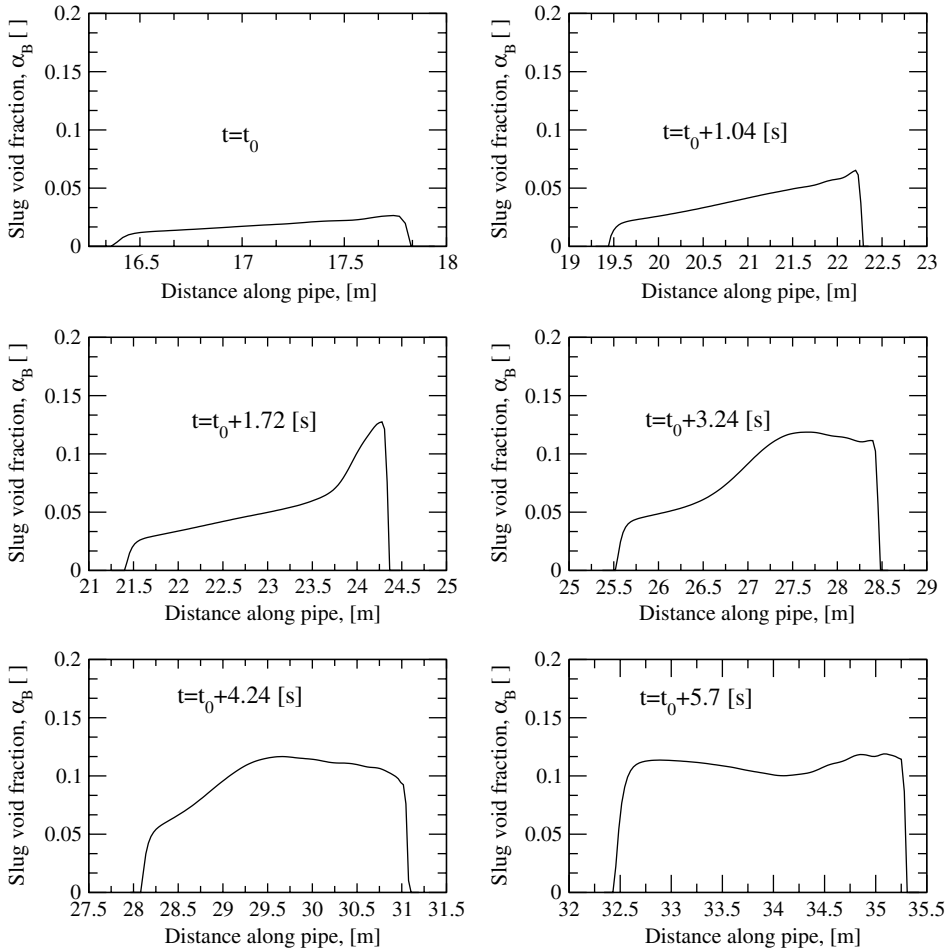

Fig. 13. Slug void fraction distribution within a slug, $U_M = 2.067$ m/s.

exhibit very similar trends for the bubble distribution. The void fraction is monitored over time for a particular slug starting from the initial conditions which correspond to stratified flow. As appears from Fig. 13, the slug voidage profile at the initial stages of entrainment shows an evident peak at the slug front, decreasing towards a minimum at the slug tail. As the length of the slug stabilises, the peak in gas bubbles at the slug front gradually levels out (through convection), until an almost uniform distribution is eventually reached. In fact, as the slugs leave the pipe, the profile appears to flatten out completely.

6.1.2. Global and film hold-up

Figs. 14 and 15 show the global and film hold-up predictions, for both aerated and un-aerated slugs, plotted against the experimental data of Manolis (1995). The predicted trends appear to be in fair agreement with the experimental measurements. While the maximum absolute discrepancies (relative to the data) for global hold-up are roughly the same (about 8.5%) for both aerated and un-

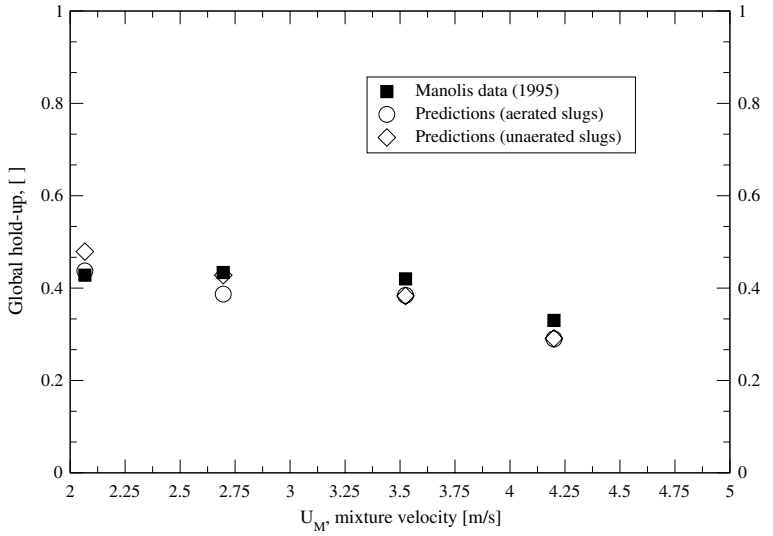

Fig. 14. Comparisons of predicted slug unit hold-up with experiments.

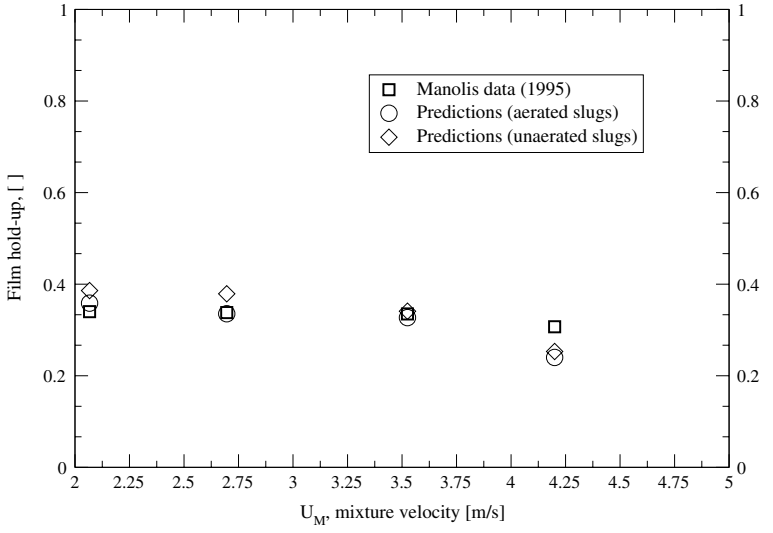

Fig. 15. Comparisons of predicted liquid film hold-up with experiments.

aerated predictions, the aerated model gives better agreement for the film hold-up (7.5% compared against 11.3%). Thus, the hold-up predictions are improved when entrainment is included but only slightly.

6.1.3. Slug frequency

Fig. 16 shows the predicted slug frequencies, with and without entrainment, compared against the data collected by Manolis (1995). The calculations fit the experimental data well. The

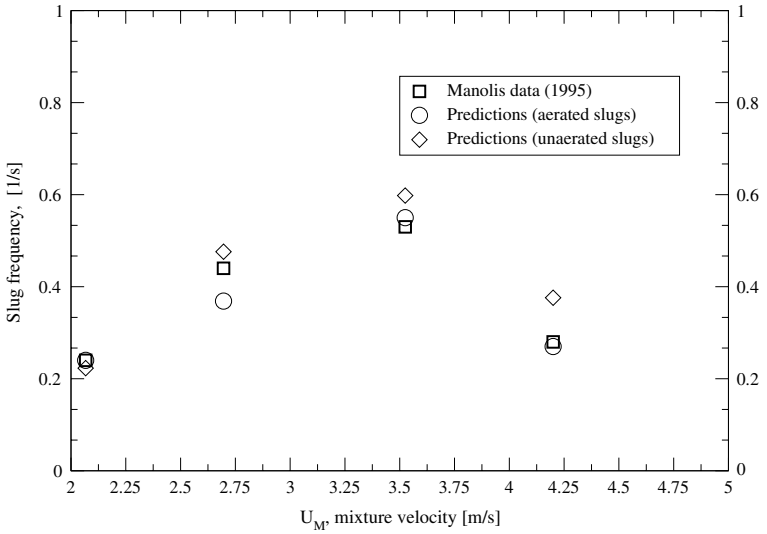

Fig. 16. Comparisons of predicted slug frequency with experiments.

discrepancies between the numerical solution and experiments are bounded, and do not exceed, for the cases studied, 16% in absolute terms. Again, the predictions accounting for gas entrainment, can be said to be more accurate than those ignoring it, although the absolute improvement is marginal (≈9%).

6.1.4. Pressure gradient

The pressure gradient along the pipe is numerically calculated, in a manner consistent with the experimental procedure followed by Manolis (1995) where two pressure transducers were located at 20.2 and 29.0 m from the pipe inlet. The measurements of the pressure differences at these locations are averaged in time as:

$$\overline{\left(\frac{\mathrm{d}p}{\mathrm{d}x}\right)} = \sum_{\mathrm{t}=t_0}^{t=t_{\mathrm{last}}} \frac{\Delta p}{\Delta x}\Delta t/(t_{\mathrm{last}} - t_0), \tag{80}$$

where $\Delta p/\Delta x$, t_0, and t_{last} represent the instantaneous pressure difference and the times when the measurements start and terminate respectively.

Fig. 17 compares the measured and predicted pressure gradients. It can be observed that the numerical calculations always under-predict the experimental values, with a discrepancy for both models (with and without entrainment) of about 25%. It should be noted that previous computations for un-aerated slugs consistently under-predicted the data obtained from the same experimental rig. This was also found to be true when the experimental data were compared with standard pressure-gradient correlations (see Fig. 18) such as those of Lockart and Martinelli (1949), Baroczy (1965), or Olujic (1985), where the discrepancies with the predictions were found to be 7%, 15%, and 6% respectively. The suspicion therefore arises that the measurements themselves might be in error. The only correlation which gives larger pressure losses is that of Beggs and Brill (1973), but this also yields some of the highest discrepancies with the data.

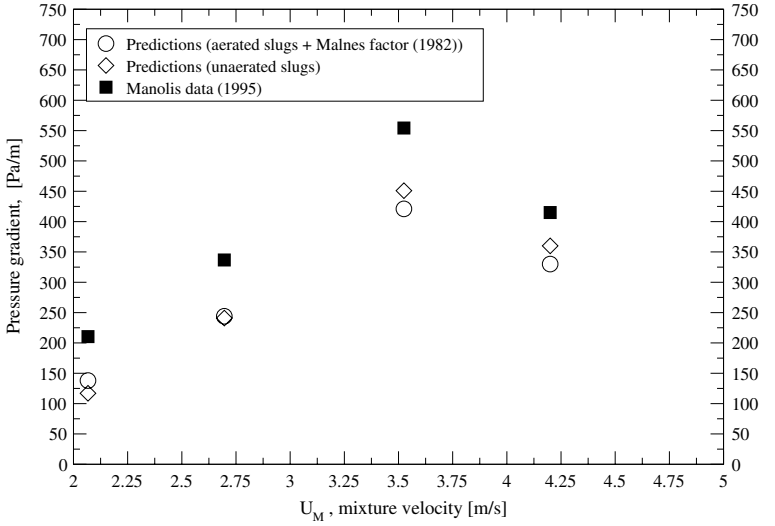

Fig. 17. Comparisons of predicted pressure gradient with experiments when the Malnes factor (1982) is accounted for.

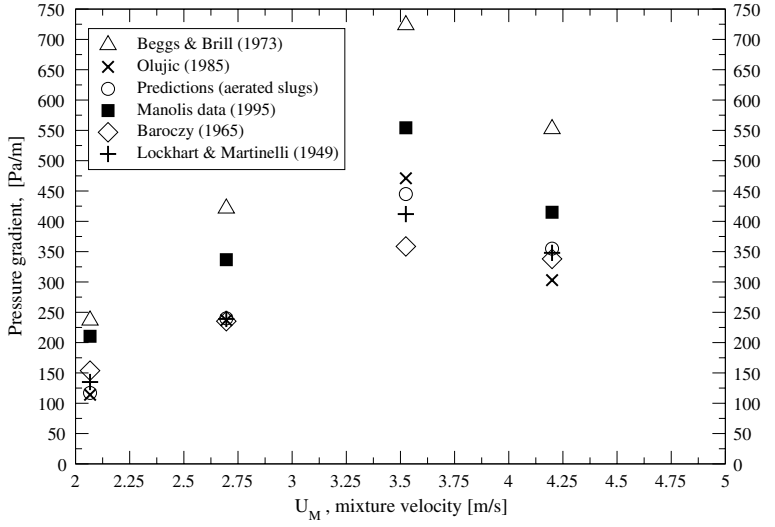

Fig. 18. Comparisons among experimental data, predictions, and some empirical correlations for pressure gradient.

6.1.5. Gas–liquid slippage

Fig. 19 shows the average slip velocity ($u_s = u_M - u_B$), expressed in cm/s, between liquid and gas in the slug body. Examination of Eq. (42), shows that the gas bubbles will travel more slowly than the liquid phase relative to the slug body, and that the slippage depends on the average pressure gradient within the slug body. For the cases studied, the numerical trend indicates that the liquid–gas slippage increases with mixture velocity up to a certain value beyond which it declines. This is

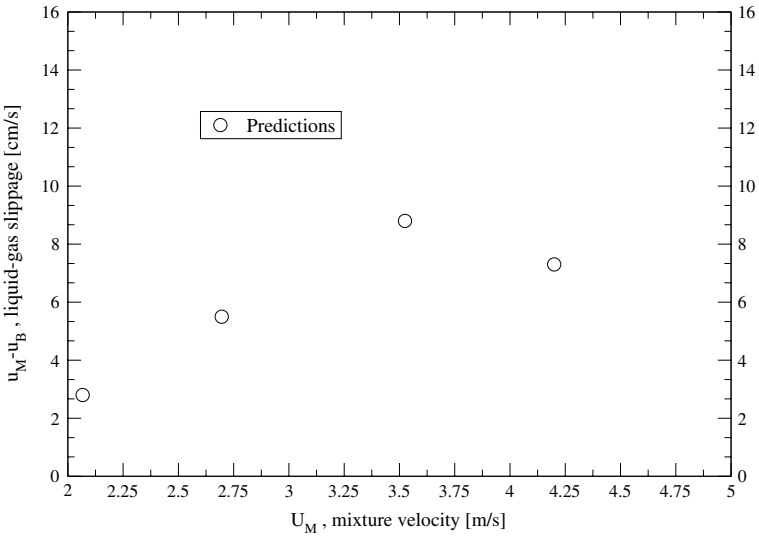

Fig. 19. Liquid–gas slippage plotted versus mixture velocity.

consistent with the trend of the computed pressure gradients, as shown in Fig. 18. When compared to the mixture velocity, the slip is quite small (typically 1–3% of the mixture velocity).

6.2. V-section

In a V-section, the mechanism that leads to slugging is largely influenced by terrain effects. This particular slug formation mechanism is mainly due to the change in the dynamics of the liquid film at the pipe dip, where the pipe changes inclination (from downwards to upwards). Since the film velocity decreases, the hold-up has to increase at the dip to conserve the mass flow of the liquid phase. The flow area of the gas is therefore reduced, and this leads to its acceleration. Since the slip between the gas and liquid becomes larger, unstable waves generate at the interface, and eventually, block the pipe cross-section forming slugs. If the flow rates are high enough, slug flow would arise from the combination of the aforementioned mechanisms (hydrodynamic and terrain induced slugging). Thus, slight terrain undulations may lead to slug formation in addition to those generated by hydrodynamic instabilities.

6.2.1. Case study

The two-phase flow of water and air in a V-section is simulated using the bubble entrainment model, and compared against the numerical results obtained by Kempf (1999) ignoring aeration. The 37 m V-section consists of a downhill section of 14 m, and an uphill section of 23 m in length (Hale, 1999). Both sections are inclined at 1.5° with respect to the horizontal. The atmospheric properties of air and water are used (the outlet pressure is fixed to atmospheric). Standard steady boundary conditions are used: fixed flow rates and liquid hold-up at the pipe inlet are assumed, and the initial conditions correspond to a uniform stratified flow. Table 2 summarises the three different cases considered, in terms of the superficial velocities U_G and U_L. Both superficial ve-

Table 2
Superficial velocities for V-section cases

Case	U_G (m/s)	U_L (m/s)
1	6.0	0.6
2	8.0	0.8
3	10.0	1.0

locities increase with ascending case number. Although the correlation provided by the hydraulic jump studies (Eq. (50)) performed better than the others for the cases previously investigated, it could not be applied to the V-section geometry owing to the high mixture velocities considered that would lead to Froude numbers larger than the upper limit ($Fr < 30$) for which the model is valid. Hence the Manolis correlation (Eq. (49)) was used instead. In what follows, the comparisons between the experimental data of Hale (1999) and predictions (with and without entrainment) for slug frequency and global hold-up will be made.

The global hold-up calculations, for both aerated and un-aerated models, are compared against the experiments in Fig. 20. The experimental data show a decrease in the hold-up with increase in mixture velocity. This trend is well captured by the computations that account for the gas entrainment, whereas the standard model shows an opposite trend to the data, in that the hold-up always increases with mixture velocity. The predictions with the entrainment model reflect the physics of the flow in a better way due to the lower slug liquid fractions calculated with aeration. Figs. 21 and 22 show the predicted dimensionless slug sizes and slug voidages versus mixture velocity. The calculated slug body lengths are in the typical range between 10 and 35 pipe diameters and it is apparent that, if the concentration of gas bubbles is appreciable, the slug liquid hold-up will be dramatically affected. The slug void fractions increase with mixture velocity (see Fig. 22) from 28% for the case of lowest mixture velocity, up to a value of 37% for the highest

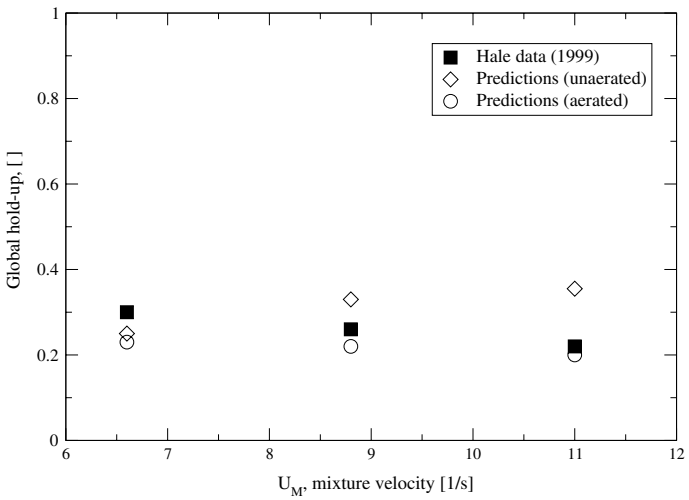

Fig. 20. Mean hold-up versus mixture velocity: comparisons between predictions and experiments for V-section cases.

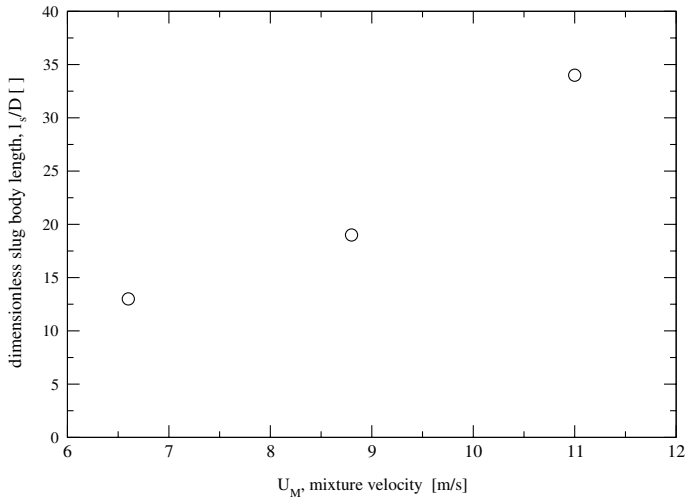

Fig. 21. Dimensionless slug body length versus mixture velocity for V-section cases.

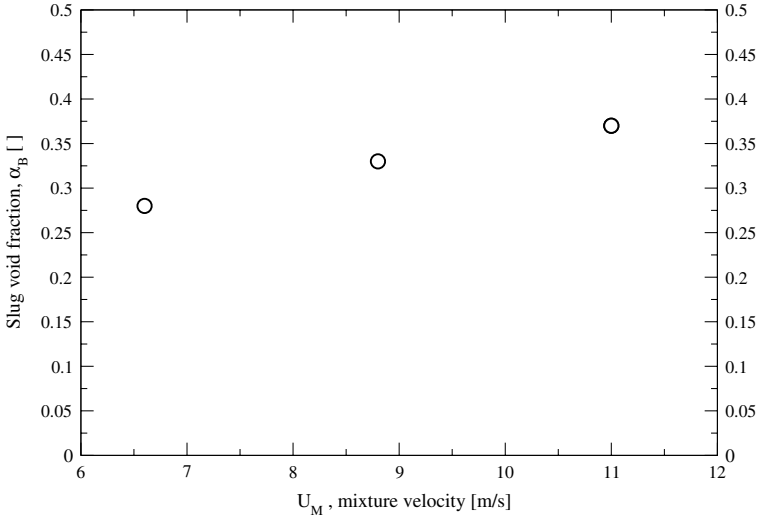

Fig. 22. Slug void fraction versus mixture velocity for V-section cases.

velocity. The high gas concentrations in the slug body clearly decrease the liquid concentration, and this explains the correct trend of the mean hold-up as calculated by the entrainment model (Fig. 20).

Fig. 23 shows the predicted and measured slug frequency against mixture velocity. The discrepancies between predictions and experiment decrease from a maximum of 38% when the entrainment is ignored to 12.5% when entrainment is accounted for. In general, the trend predicted by both models is in fair agreement with the experiments, since both predict an increase in slug frequency with increase in mixture velocity.

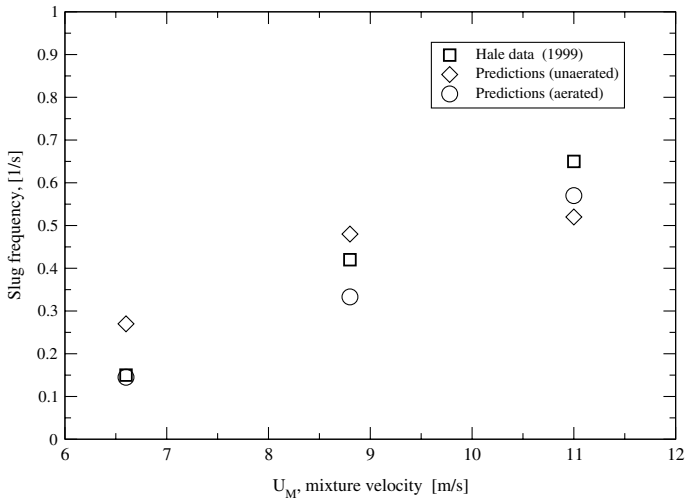

Fig. 23. Slug frequency: comparisons between predictions and experiments for V-section cases.

It is apparent that the aeration model has more of an impact on the quality of the predictions in the V-section flow than in the preceding studies of the flow in horizontal pipes. This is probably due to the higher void fractions in slugs encountered in the V-section flows which would then exert an appreciable influence on the dynamics of the slug; lower fractions of entrained gas seem not to have much influence, at least for the cases studied.

7. Conclusion

A model accounting for the aeration phenomenon in horizontal and nearly horizontal two-phase slug flow has been developed and implemented in the framework of the transient one-dimensional two-fluid model. The bubble volume concentration is calculated by means of a transport scalar equation. Closure models for the determination of the slug front and tail velocities, and for the calculation of the rate of entrainment at the slug front are incorporated; these are based on existing correlations. The model was assessed against some available experimental data for air–water two-phase slug flow in a horizontal pipe and in a V-section. The model improves the accuracy of predictions for liquid hold-up and slug frequency, compared to those ignoring entrainment. However, it was found that the improvement was somewhat marginal at least for the cases of horizontal pipes studied here. Where an appreciable effect was observed was in the case of V-section flow. There, previous erroneous predictions of the trend in hold-up are rectified. This could very well be due to the higher void fractions encountered in the latter case, which would have more of an influence on the slug flow characteristics than when the slug voidage is low. More exhaustive studies on other pipe configurations and involving wider flow conditions and different fluids are therefore necessary before making more definitive conclusions as to when the entrainment phenomenon becomes a dominant factor in determining the characteristics of slug flow.

Acknowledgements

This work has been undertaken within the second stage of the Transient Multiphase Flows' Co-ordinated Research Project. The authors wish to acknowledge the contributions made to this project by the Engineering and Physical Sciences Research Council (EPSRC) and to the following industrial organisations: ABB; AEA Technology; BG International; BP Exploration; Chevron; Conoco; Enterprise Oil; Granherne; Institutt for Energiteknikk; Institut Francais du Petrole; Marathon Oil; Mobil North Sea; Norsk Hydro; Scandpower; TotalFinaElf.

The authors also wish to thank Prof. G.F. Hewitt, his team and colleagues in the Department of Chemical Engineering at Imperial College, not only for the provision of experimental data, but also for the numerous discussions which had shed much light on the physics of the entrainment phenomenon.

References

Abdul-Majeed, G.H., 2000. Liquid slug hold-up in horizontal and slightly inclined two-phase slug flow. J. Petr. Sci. Eng. 27, 27–32.

Andreussi, P., Bendiksen, K., 1989. An investigation of void fraction in liquid slugs for horizontal and inclined gas–liquid pipe flow. Int. J. Multiphase Flow 15, 937–946.

Andreussi, P., Bendiksen, K., Nydal, O.J., 1993. Void distribution in slug flow. Int. J. Multiphase Flow 19, 817–828.

Banerjee, S., Chan, A.M.C., 1980. Separated flow models-I: analysis of the averaged and local instantaneous formulations. Int. J. Multiphase Flow 6, 1–24.

Baroczy, C.J., 1965. A systematic correlation for two-phase pressure drop. In: CEP Symp. Ser., vol. 62, p. 232.

Beggs, H.D., Brill, J.P., 1973. Study of two-phase flow in inclined pipes. J. Petr. Tech. 25, 607–617.

Bendiksen, K.H., 1984. Experimental investigation of the motion of long bubbles in inclined tubes. Int. J. Multiphase Flow 10, 467–483.

Bendiksen, K.H., Malnes, D., Nydal, O.J., 1996. On the modelling of slug flow. Chem. Eng. Comm. 142, 71–102.

Bonetto, F., Lahey, R.T., 1993. An experimental study on air carry under due to a plunging jet. Int. J. Multiphase Flow 19, 281–294.

Bonizzi, M., 2003. Transient One-dimensional Modelling of Multiphase Slug Flows. PhD Thesis, Imperial College London, UK.

Bonizzi, M., Issa, R.I., Kempf, M.H.W., 2001. Modelling of gas entrainment in horizontal slug flow. In: 4th Int. Conf. Multiphase Flow, ICMF2001, New Orleans, LA, US.

Chanson, H., 1996. Air Bubble Entrainment in Free-surface Turbulent Shear Flow. Academic Press.

Chun, M.H., Sung, C.K., 1996. Onset of slugging criterion based on characteristics and stability analyses of transient one-dimensional two-phase flow equations of the two-fluid model. Int. Comm. Heat Mass Transfer 23, 473–484.

Dukler, A.E., Hubbard, M.G., 1975. A model for gas–liquid slug flow in horizontal and near horizontal tubes. I&EC Fundam. 14, 337–347.

Fabre, J., Liné, A., 1992. Modelling of two-phase slug flow. Annu. Rev. Fluid Mech. 24, 21–46.

Fan, Z., Lusseyrun, F., Hanratty, T.J., 1993. Initiation of slugs in horizontal gas–liquid flows. J. AIChE 39, 1741–1753.

Fernandes, R.C., Semiat, R., Dukler, A.E., 1983. Hydrodynamic model for gas–liquid slug flow in vertical tubes. J. AIChE 29, 981–989.

Ferschneider, G., 1983. Ecoulements gaz–liquide à poches et à bouchons en conduite. Revue de l'Institut Français du Pétrole 38, 153–182 (in French).

Gregory, G.A., Nicholson, M.K., Aziz, K., 1978. Correlation of the liquid volume fraction in the slug for horizontal gas–liquid slug flow. Int. J. Multiphase Flow 4, 33–39.

Grotjahn, K., Mewes, D., 2001. Measurements and calculations on the transient behaviour of two-phase slug flow in a horizontal pipe. In: 4th Int. Conf. Multiphase Flow, ICMF2001, New Orleans, LA, US.

Hale, C.P., 1999. Slug flow in a V-section. Private Communication, Imperial College, London, UK.
Hand, N.P., 1991. Gas–Liquid Co-current Flow in a Horizontal Pipe. PhD Thesis, Queen's university, Belfast.
Hirsch, C., 1988. In: Numerical Computation of Internal and External Flow, vol. 1. John Wiley and Sons, New York.
Ishii, M., 1975. Thermo-fluid Dynamic Theory of Two-phase Flows. Eyrolles, Paris.
Ishii, M., 1978. One-dimensional drift-flux model and constitutive equations for relative motion between phases in various two-phase flow regimes. Report ANL-77-47, Argonne National Laboratory, Argonne, IL, US.
Ishii, M., Mishima, K., 1984. Two-fluid model and hydrodynamic constitutive relations, Nucl. Eng. Design 82, 107–126.
Issa, R.I., Abrishami, Y., 1986. Computer modelling of slugging flow. Technical Report, Imperial College London, UK.
Issa, R.I., Woodburn, P.J., 1998. Numerical prediction of instabilities and slug formation in horizontal two-phase flows. Proc. Third Int. Conf. on Multiphase Flow, Lyon.
Issa, R.I., Kempf, M.H.W., 2003. Simulation of slug flow in horizontal and nearly horizontal pipes with the two-fluid model. Int. J. Multiphase Flow 29, 69–95.
Jepson, W.P., 1987. The flow characteristics in horizontal slug flow. In: Proc. of 3rd Int. Conf. Multiphase Flow, The Hague, The Netherlands, pp. 187–198.
Jones, A.V., Prosperetti, A., 1985. On the suitability of first-order differential models for two-phase flow predictions. Int. J. Multiphase Flow 11, 133–148.
Kempf, M.H.W., 1999. Simulation of slug flow in a V-Section. Interim Report, Imperial College, London, UK.
Lockart, R.W., Martinelli, R.C., 1949. Proposed correlation of data for isothermal two-phase, two-component flow in pipes. Chem. Eng. Prog. 45, 39–48.
Malnes, D., 1982. Slug flow in vertical, horizontal and inclined pipes. V. Inst. for Energy Tech., Kjeller, Norway Report IFE/KR/E-83/002.
Manolis, I.G., 1995. High Pressure Gas–Liquid Slug Flow. PhD Thesis, Imperial College, London, UK.
Nydal, O.J., Andreussi, P., 1991. Gas entrainment in a long liquid slug advancing in a near horizontal pipe. Int. J. Multiphase flow 17, 179–189.
Nydal, O.J., Banerjee, S., 1996. Dynamic slug tracking simulations for gas–liquid flow in pipelines. Chem. Eng. Comm. 141–142, 13–39.
Olujic, Z., 1985. Predicting two-phase flow friction loss in horizontal pipes. Chem. Eng. 92, 45–50.
Paglianti, A., Trotta, G., Andreussi, P., Nydal, O.J., 1992. The effect of fluid properties and geometry on void distribution in slug flow. In: 6th Int. Conf. Multiphase Production, Cannes, France, pp. 193–203.
Rajaratnam, N., 1967. Hydraulic jumps. Adv. Hydrosci. 4, 197–280.
Spedding, P.L., Hand, N.P., 1997. Prediction in stratified gas–liquid co-current flow in horizontal pipelines. Int. J. Heat Mass Transfer 40, 1923–1935.
Taitel, Y., Dukler, A.E., 1976. A model for predicting flow regime transitions in horizontal and near horizontal gas–liquid flow. AIChE J. 22, 47–55.
Tomiyama, A., Kataoka, I., Fukuda, T., Sakaguchi, T., 1995. Drag coefficient of bubbles (2nd report, drag coefficient for a swarm of bubbles and its applicability to transient flow). Trans. Jpn. Soc. Mech. Eng. B, 46–53.
Wallis, G.B., 1969. One-dimensional Two-phase Flow. McGraw-Hill.
Wisner, P., 1965. On the role of the Froude criterion for the study of air entrainment in high velocity flows. In: Proc. 11th IAHR Congress, Leningrad, USSR, paper 1.15 (in French).
Zuber, N., Findlay, J.A., 1965. Average volumetric concentration in two-phase flow systems. J. Heat Transfer, 453–468.